

Boundary effects of molecular diffusion in nanoporous materials: a pulsed field gradient nuclear magnetic resonance study

Oliver Geier, Randall Q. Snurr, Frank Stallmach, Jörg Kärger

ABSTARCT

The boundary conditions of intraparticle diffusion in nanoporous materials may be chosen to approach the limiting cases of either absorbing or reflecting boundaries, depending on the host-guest system under study and the temperature of measurement. Pulsed field gradient nuclear magnetic resonance (PFG NMR) is applied to monitor molecular diffusion of *n*-hexane and of an *n*-hexane – tetrafluoromethane mixture adsorbed in zeolite crystallites of type NaX under either of these limiting conditions. Taking advantage of the thus established peculiarities of mass transfer at the interface between the zeolite bulk phase and the surrounding atmosphere, three independent routes for probing the crystal size are compared. These techniques are based on (i) the measurement of the effective diffusivity under complete confinement, (ii) the application of the so-called NMR tracer desorption technique and (iii) an analysis of the time dependence of the effective diffusivity in the short-time limit where, by an appropriate variation of the adsorbate and the measuring conditions, the limiting cases of reflecting and adsorbing boundaries could be considered. All these techniques are found to yield coinciding results, which are in excellent agreement with the crystal sizes determined by microscopy.

I. INTRODUCTION

Molecular diffusion is among the celebrated topics of current research of nanoporous materials¹⁻³. The reasons for this include (i) the key role of diffusion in numerous practically important processes like chemical separations and catalysis^{1,4}, (ii) the multitude of basic phenomena of fluid – solid interaction appearing in the features of molecular propagation^{2,5} and (iii) the intriguing discrepancy between the results of various experimental techniques^{1,3,4,6}. It is in particular due to the introduction of pulsed field gradient nuclear magnetic resonance (PFG NMR) to diffusion studies with nanoporous materials, that in the last few years our knowledge about the guest mobility in nanoporous materials has been substantially improved⁴.

Equally important from a practical point of view and probably even more demanding with respect to its relevance for fundamental research, however, is the process of molecular exchange between the adsorbate phase and the surrounding atmosphere. So far, research of this topic has mainly involved theoretical studies of the rate of sorbate release from the intracrystalline space⁷⁻⁹. Analysing the elementary processes of molecular uptake, in ref.¹⁰ also the reverse process has been considered. In this way, e.g., for zeolite ZSM-5 in an atmosphere of toluene a “sticking” probability of the order of 10^{-7} (corresponding to a rejection probability of $(1 - 10^{-7})$) has been estimated. Dynamic equilibrium between the adsorbate and gaseous phases implies that molecular escape rate from intracrystalline space into the surrounding atmosphere has to be of a similar, incredibly small magnitude.

Being sensitive to the distribution of molecular displacements (and not only to its second moment)^{4,11,12}, PFG NMR is able to discriminate between those molecules which leave the

individual particles during the observation time and those which are reflected into their interior. In this way, PFG NMR has the potential to provide direct information about the rejection rate of molecules encountering the particle surface from inside. Using the principle of dynamic equilibrium, this information may be likewise used to estimate the sticking rate of molecules encountering the particle surface from the gas phase. Studies of this type are complicated, however, by the fact that the experimentally observable effect of the rejection probability most decisively depends on the considered length of the diffusion step to which the rejection probability is referred to ^{7,8}. It may in particular be shown that for any finite constant rejection rate < 1 , the experimentally observable behaviour becomes indistinguishable from that of rejection probability 0, if only the length of the diffusion step is considered to be sufficiently small ⁷. Provided that upon leaving the particle, the guest molecule fades out of observation for diffusion steps much smaller than the totally covered diffusion paths, the existence of a finite rejection rate < 1 (just like rejection rates equal to 0) would be adequately reflected by subjecting the diffusion problem to the boundary conditions of an absorbing wall ¹³. Only with rejection rates equal to 1, intraparticle diffusion can be considered to proceed under confinement by reflecting walls, following the shape of the particle surface.

The concept of step-wise molecular propagation is nothing more than a – rather productive – model assumption. In this context, also the escape rate from intraparticle space into the surrounding atmosphere, being defined on the basis of such a step model, cannot be expected to be anything else than a model parameter. Its physical significance depends on the chosen step length.

Using a mesoscopic perspective, molecular exchange at the particle boundary may be quantified to a much better extent by introducing a transmission probability ρ defined by the appropriately chosen boundary condition of intracrystalline diffusion

$$D_0 \vec{n} \text{ grad} P(\vec{r}, \vec{r}', t) + \rho P(\vec{r}, \vec{r}', t) /_{\vec{r} \in \Sigma} = 0. \quad (1)$$

$P(\vec{r}, \vec{r}', t)$ denotes the probability density (the so-called propagator^{4,11,14} that a molecule starting at position \vec{r} at time 0 shall have got to \vec{r}' at time t , where \vec{r} is a position in the particle surface. D_0 is the intraparticle diffusivity and \vec{n} denotes the unit vector normal to the particle surface at position \vec{r} . Within the above considered model, the transmission probability ρ represents the escape probability per time unit and step length.

In diffusion studies using PFG NMR the physical significance of the transmission probability ρ as introduced by Eq. (1) may appear in essentially two different ways. As a first option, Eq. (1) may be considered to describe a PFG NMR experiment in the case of completely confined diffusion, as soon as signal intensity is lost as a consequence of nuclear magnetic relaxation in the boundaries. In this case, ρ denotes the surface relaxivity. This is the usual situation, one is confronted with on considering fluids within the pores of rock. Refs.¹⁵ provide an excellent theoretical framework for their interpretation.

A second option is related to the interrelation of the rates of the intracrystalline diffusivity (D_{intra}) and the so-called long-range diffusivity $D_{\text{l.r.}}$. The latter quantity is approached by the product $p_{\text{inter}} D_{\text{inter}}$ of the relative amount of molecules in the interparticle space and their diffusivity¹⁶. Let us first consider the condition $D_{\text{intra}} \ll D_{\text{l.r.}}$. Since generally the activation energy of intracrystalline diffusion is much smaller than the heat of adsorption, for most

systems this condition may be easily fulfilled by choosing sufficiently large temperatures. If there are no additional transport resistances at the outer surface of the particles, molecules encountering the particle surface will soon dissipate over the whole space. In the PFG NMR experiment their contribution to the signal may be easily separated from that of the molecules that have not encountered the surface and are still within the particles. Considering only these latter molecules, we have exactly the same situation as with absorbing boundaries¹⁷. If - on the other hand- molecular exchange with the surroundings is excluded by either additional transport resistances at the surface (“surface barriers”) or by an extremely low rate of molecular transport through the bed of particles (generally to be ensured at sufficiently low temperatures), diffusion is essentially confined to the intraparticle space, so that now the particle surface acts as a reflecting wall. We make use of these two experimental options in the present communication.

Following a few investigations that have applied aspects of this theory to the interpretation of PFG NMR diffusion measurements with nanoporous materials¹⁸, the present communication provides a first complete analysis of PFG NMR diffusion measurements with nanoporous materials. The cases of both reflecting and absorbing boundaries are considered and compared with the results of two further, independent techniques of PFG NMR analysis, viz. the measurement under the conditions of completely restricted diffusion and the so-called NMR tracer desorption technique.

II. EXPERIMENTAL

Figure 1 gives an overview of the specimen of zeolite NaX applied in this study. The zeolite crystallites were synthesized using triethylamine and were kindly provided by George T. Kokotailo. The distribution curve of the crystal radii given in Fig. 1(b) represents the (crystal) volume-weighted probabilities, which coincide with the probability that a guest molecule within the sample resides in a crystal of radius r . The radii r are effective quantities, resulting from the crystal surface S and volume V via the relation $3V/S$. The subsequent discussion of the NMR experiments implies different ways of averaging over the sample sizes. The following mean values shall be of particular interest:

$$\langle R^2 \rangle^{1/2} \equiv \left(\int_0^{\infty} p(R) R^2 dR \right)^{1/2} = 11.6 \mu\text{m} \quad (2a)$$

$$\langle \frac{1}{R} \rangle^{-1} \equiv \left(\int_0^{\infty} p(R) / R dR \right)^{-1} = 10.9 \mu\text{m} \quad (2b)$$

$$\langle \frac{1}{R^2} \rangle^{-1/2} \equiv \left(\int_0^{\infty} p(R) / R^2 dR \right)^{-1/2} = 10.5 \mu\text{m} \quad (2c)$$

The average of the three values is, thus, $11.0 \pm 0.5 \mu\text{m}$. It shall turn out that the differences between these values are of the order of the uncertainty of the results stemming from the different applications of PFG NMR.

For the PFG NMR diffusion measurements about 200 mg of the NaX zeolites were introduced into 7.8 mm outer diameter NMR tubes. The zeolites were activated by increasing the temperature at a rate of about 10 K/h under continuous evacuation until the samples reached a

final temperature of 673 K where they were kept for additional 20 h at a pressure of less than about 5×10^{-3} mbar. After cooling to room temperature, a controlled amount of the guest molecules were introduced by freezing them into the sample from a calibrated volume. In this way, we prepared a sample containing only *n*-hexane at a loading of 2 molecules per supercage and a second sample containing *n*-hexane and tetrafluoromethane, each at a loading of 1 molecule per supercage (two component adsorption). After introduction of the adsorbates, the samples have been fused and stored for several weeks so that the guest molecules could equilibrate over the sample before measurement.

The diffusion measurements were carried out at a proton resonance frequency of 400 MHz (*n*-hexane) and a fluorine resonance frequency of 376.4 MHz (tetrafluoromethane) using the home-built NMR spectrometer FEGRIS 400 NT¹⁹. The spectrometer is equipped with a ultra-high intensity pulsed field gradient facility consisting of an actively shielded Anti-Helmholtz gradient coil and two Techron gradient current amplifiers connected in push-pull-configuration¹⁹. In order to circumvent the possibly disturbing influence of internal field gradients, the 13-interval pulse sequence with alternating pulsed field gradients was employed²⁰. The width δ of the pulsed field gradients was chosen to be 0.4 ms, the duration 2τ of the “dephasing” and “read” intervals (separation between the first two $\pi/2$ pulses and between the last $\pi/2$ pulse and the signal (“echo”) maximum, respectively) was set to 1.2 ms. The amplitude g of the field gradient pulses was varied between 0.1 and 8.5 T/m. The time Δ between the two pairs of alternating gradient pulses covered a range from 1.6 ms up to 20 ms. The accuracy of temperature control in the measurements was of the order of ± 0.5 K.

III. RESULTS AND DISCUSSION

A. Restricted Diffusion

Compared to other experimental techniques applied to diffusion studies in nanoporous materials, PFG NMR is distinguished by a number of advantages including its non-invasive character and the possibility to vary the observation scales from microscopic to mesoscopic dimensions^{4,5,11,12}. The latter option provides a straightforward means for an independent check of the validity of the obtained diffusion data. Provided that molecular propagation during the observation time of the PFG NMR experiment is confined to the individual crystallites, the maximum molecular displacements have to be a sole function of the crystal size. Thus, for crystallites approaching the shape of a sphere of radius R , the effective diffusivity D_{eff} resulting from the PFG NMR experiment in the limit of large observation times $t = \Delta$, is found to obey the simple relation^{4,5,11,12}

$$D_{\text{eff}} = R^2 / (5t). \quad (3)$$

The effective diffusivity D_{eff} of the PFG NMR experiments is related to the mean square displacement $\langle r^2(t) \rangle$ of the molecules under study during the observation time t via

$$D_{\text{eff}} = \langle r^2(t) \rangle / (6t) \quad (4)$$

which in the case of normal, unrestricted diffusion coincides with the Einstein relation, with D_{eff} becoming the genuine diffusivity of the system. The effective diffusivity D_{eff} follows

immediately from the PFG NMR attenuation curve $\Psi(q, t)$ of the spin echo, whose dependence in the limit of small gradient pulse intensities obeys the relation

$$\lim_{q \rightarrow 0} \Psi(q, t) = \exp(-q^2 D_{\text{eff}} t) \quad (5)$$

with q denoting the intensity parameter of the field gradient pulses (sometimes referred to as a generalized scattering vector). In the limit of small pulse widths and small separations between the two pulses of the bipolar pulse pair in the 13-interval pulse sequence (i.e., for $\delta, \tau \ll \Delta$), q is given by

$$q = \gamma(2\delta)g \quad (6)$$

with γ denoting the gyromagnetic ratio.

The excellent agreement between the root mean square displacements determined by PFG NMR under the condition of completely restricted diffusion and the crystal size has repeatedly served as an independent check of the reliability of the PFG NMR diffusivity data on zeolitic diffusion⁴. In the present study the conditions of restricted diffusion are ideally fulfilled for *n*-hexane. At room temperature the long-range diffusivity of *n*-hexane in NaX is at least 2 orders of magnitude smaller than the intracrystalline diffusivity²¹. This is an immediate consequence of the large heat of adsorption (≈ 80 kJ/mol)²², acting as an activation energy of long-range diffusion. Molecular escape from the intracrystalline space into the surrounding atmosphere is therefore practically excluded. Figure 2 displays the PFG NMR signal attenuation curves measured at observation times of 500 and 800 ms. Analysing

these data on the basis of Eqs. (3) and (5) leads to effective diffusivities of $5.42 \times 10^{-11} \text{ m}^2\text{s}^{-1}$ and $3.55 \times 10^{-11} \text{ m}^2\text{s}^{-1}$ with the corresponding (volume-weighted) root mean square crystal radii of $11.6 \text{ }\mu\text{m}$ and $11.9 \text{ }\mu\text{m}$, respectively. These values are in good agreement with the value of $11.6 \text{ }\mu\text{m}$ determined microscopically via Eq. (2a).

B. NMR Tracer Desorption

The NMR tracer desorption technique^{4,23} is applied under exactly the opposite situation as considered in section III A, i.e. with long-range diffusivities $D_{l,r} = p_{\text{inter}}D_{\text{inter}}$ significantly exceeding the intracrystalline diffusivities D_{intra} . Now, molecules encountering the crystallite surface during the observation time t will cover much longer distances through the bed of crystallites than they would have in the intracrystalline space. In the representation of the PFG NMR spin echo attenuations in Fig. 3, these molecules give rise to the first steep decay. Having in mind that these molecules undergo much larger displacements, this steep decay is an immediate consequence of Eq. (5) with D_{eff} given by the long-range diffusivity. As expected, the relative contribution of the fast decaying part to the signal (i.e., the relative number of molecules leaving their crystallites during t) is increasing with the observation time t . In comparison with section IIIA, in the present analysis also gradient pair distances are considered for which the long-time limit cannot be applied anymore. Therefore, the abscissa of Fig. 3 is scaled in terms of

$$[\gamma(2\delta)g]^2(\Delta - \tau/2 - \delta/6) = [\gamma(2\delta)g]^2 t \quad (7)$$

which – taking account of the more general case - has to replace q^2t in Eq. (5)²⁰. With Eq. (5) one finds easily that in the long-time limit the abscissa notation of Fig. 3 coincides with the simpler notation chosen in section IIIA.

Figure 4 displays the relative contribution $\gamma(t)$ of the second, more slowly decaying part of the spin-echo attenuation curve as presented in Fig. 3 for the five (effective) observation times $t \equiv (\Delta - \tau/2 - \delta/6) = 1.63, 3.63, 5.63, 7.63$ and 14.63 ms. This curve represents the relative fraction of molecules which after time t have not yet left the crystallites in which they have been at time $t = 0$. Since such information is typically provided by conventional tracer desorption experiments, this special type of application of PFG NMR has been termed NMR Tracer Desorption or - owing to the much smaller time scale - “Fast Tracer Desorption”^{4,23}.

Figure 4 shows the experimentally observed NMR tracer desorption curve of tetrafluoromethane in the specimen of NaX zeolite. Clearly, $\gamma(t)$ decreases with increasing t since more and more tetrafluoromethane molecules encounter the crystallite boundary with increasing t and are, obviously, allowed to pass through it into the intercrystalline gas phase. The analytical expression for diffusion-limited tracer desorption depends on crystallite size and shape. For mono-disperse spherical crystallites of radius R one obtains^{3,4}

$$\gamma(t) = \sum_{n=1}^{\infty} \frac{6}{n^2 \pi^2} \exp\left(-n^2 \pi^2 t \frac{D_0}{R^2}\right). \quad (8a)$$

In the case of a size distribution of spherical crystallites ($p(R)$) Eq. (8a) is modified to

$$\gamma(t) = \int_0^{\infty} p(R) \sum_{n=1}^{\infty} \frac{6}{n^2 \pi^2} \exp\left(-n^2 \pi^2 t \frac{D_0}{R^2}\right) dR. \quad (8b)$$

The full line in Fig. 4 represents the fit of Eq. (8a) to the experimental values of the tracer desorption. For the ratio D_0/R one obtains a value of 0.873 s^{-1} . With a value of $D_0 = 4.17 \times 10$

$^{-10} \text{ m}^2 \text{ s}^{-1}$, which in section III C shall be shown to represent the best experimental value for the intracrystalline diffusivity, one obtains a radius of $R = 10.7 \text{ } \mu\text{m}$ which is in good agreement with the value of $11.0 \text{ } \mu\text{m}$ resulting from Eq. (2c). The dashed line in Fig. 4 represents the forward modelling of Eq. (8b) where we used the size distribution known from SEM (Fig. 1) and the D_0 of $4.17 \times 10^{-10} \text{ m}^2 \text{ s}^{-1}$ as parameter. Both models for the tracer desorption are in very good agreement with the experimental data, showing that the crystallite size and the intracrystalline diffusion control the exchange of tetrafluoromethane through the NaX crystallites.

C. Short-Time Limit of the Effective Diffusivity

From the very beginning of the applications of PFG NMR to diffusion measurements in zeolites⁴, mean diffusion paths $\langle r^2(t) \rangle^{1/2}$ during the time t of the PFG NMR experiment have been required to be smaller than the crystal size as a necessary and sufficient supposition for obtaining genuine intracrystalline diffusivities. Recent progress in the PFG NMR instrumentation and the thus obtained enhanced sensitivity have made it possible that today even in this short-time limit of PFG NMR more profound information may be deduced^{18,19,24}. The analysis is based on the formalism developed by Mitra and co-workers¹⁵, which was originally derived for pore fluids. In the given context of beds of zeolites in equilibrium with a gas phase, as a consequence of the generally negligible contribution of the gas phase to the signal, the roles of the pore fluid and of the pore walls in refs.¹⁵ are assumed by the intracrystalline phase of guests in the zeolite crystallites and the crystal surface, respectively. Again approximating the crystal shape by spheres of radius R , the dependence of the effective diffusivities as defined by Eq. (5) up to second order results to be¹⁵

$$\frac{D(t)}{D_0} = 1 - \frac{4}{3R} \left(\frac{D_0 t}{\pi} \right)^{1/2} + \frac{1}{2R^2} D_0 t \quad (9)$$

and

$$\frac{D(t)}{D_0} = 1 - \frac{2}{3R} \left(\frac{D_0 t}{\pi} \right)^{1/2} + \frac{1}{R^2} D_0 t \quad (10)$$

for a reflecting (as considered in section IIIA) and an absorbing (as considered in section III B) crystal surface, respectively. $D_0 \equiv D(t=0)$ denotes the genuine intracrystalline diffusivity.

As an example for the primary data obtained in this study and their accuracy, Fig. 5 displays the spin-echo attenuation curves for *n*-hexane at 298 K for three effective observation times $t = 1.63$ ms; 4.83 ms and 8.63 ms. Following the discussion of section III A, the physical situation of these experiments corresponds to that of reflecting boundaries. The effective diffusivities $D(t)$ are taken from the (initial) slope of these curves as required by Eq. (5).

In contrast, for the tetrafluoromethane fraction, which remains during t in the individual crystallites (situation considered in section III B), the case of absorbing boundaries (Eq. (10)) applies. The corresponding effective diffusivities are determined from the slope of the second, less steep decay of the spin-echo attenuation curves displayed in Fig. 3.

Figure 6 represents these relative effective diffusivities $D(t)/D_0$ as function of $\sqrt{D_0 t}$ together with the best fits of Eqs. (9) and (10), respectively, with D_0 and R as fitting parameters. The molecules under study were *n*-hexane under single-component adsorption ($T = 298$ K, (O)) and *n*-hexane ($T = 298$ K, (Δ)) and tetrafluoromethane ($T = 203$ K, (□)) under two-component adsorption. The temperatures were chosen to yield values of $(D_0 t)^{1/2}$ as small as

possible. As discussed in sections III A and B, the measuring conditions for *n*-hexane correspond to reflecting (Eq. (9)) and for tetrafluoromethane to absorbing (Eq. (10)) boundary conditions. The values of the genuine intracrystalline diffusivities D_0 and the crystallite radii obtained by the fitting procedure are summarized in Table I. Moreover, Table I also includes the ratios O(2)/O(1) of the terms in second and first order of $(D_0t)^{1/2}$ in Eqs. (9) and (10), for the minimum and maximum observation times t_{\min} and t_{\max} , respectively. From this comparison it appears that the estimate in second order may in fact be expected to be sufficiently accurate, while a first-order estimate would still lead to substantial deficiencies.

	$D_0 / \text{m}^2\text{s}^{-1}$	$R / \mu\text{m}$	$(\text{O}(2)/\text{O}(1))_{t_{\min}}$	$(\text{O}(2)/\text{O}(1))_{t_{\max}}$
2 <i>n</i> -hexane/cav., single component adsorption, 298 K	3.53×10^{-10}	9.1	0.080	0.196
1 <i>n</i> -hexane/cav., two- component adsorption, 298 K	5.54×10^{-10}	7.8	0.070	0.197
1 tetrafluoromethane/cav., two- component adsorption, 203 K	4.17×10^{-10}	9.1	0.240	0.721

Table I. Estimate of the genuine intracrystalline diffusivities (D_0) and the crystal radii (R) by PFG NMR data analysis on the basis of the Mitra formalism (Eqs. (9) and (10) and Refs. ¹⁵). The two last columns represent the ratio of the contributions in second and first order in Eqs. (9) and (10) for the shortest and largest observation times considered in Fig. 6.

Again, as observed already in sections IIIA and III B by two completely different ways of analysis, satisfactory agreement is found between the NMR data and the microscopically determined value of the crystal radius. Particularly satisfactory is the fact that in the two-component sample, in which one component is subject to the conditions of absorbing and the

other to the conditions of reflecting boundaries, the correspondingly different ways of analysis yield similar mean radii. The absolute values of the diffusivities correspond to the quite generally expected behaviour^{4,25}. This refers in particular to the smaller diffusivity of the bulkier *n*-hexane molecule in comparison with tetrafluoromethane, which in the present measurements is taken into account by the higher measuring temperature for *n*-hexane, and to the slightly enhanced diffusivity of the *n*-hexane molecules on passing from the sample with 2 molecules per cavity (single-component adsorption) to the two-component sample, where one *n*-hexane molecule per cavity has been replaced by the more mobile tetrafluoromethane molecule.

IV. CONCLUSION

For the first time, the influence of the finite size of the zeolite crystallites has been simultaneously considered for one and the same sample under three different measuring conditions, viz. the condition of (i) completely restricted diffusion, of (ii) NMR tracer exchange and (iii) in the short-time limit of diffusion. The satisfactory agreement of the results obtained by each of these methods with the microscopically determined crystal sizes is a solid confirmation of the consistency of the applied methods. So far, the measurements have been carried out under the limiting conditions of either reflecting or absorbing boundaries, for which analytical expressions are readily available. The consideration of the intermediate case shall be a challenging task of future investigations both with respect to experimental procedure and theoretical analysis.

In the present study the application of ultra-high-intensity field gradient pulses permitted the measurement of effective intracrystalline diffusivities deviating from the genuine ones by but

a few percents. This is the more remarkable since the studies have been performed with medium-sized crystallites ($R \sim 10 \mu\text{m}$) rather than with extremely large ones ($R \sim 100 \mu\text{m}$) as described, e.g., in ⁴. In this way, by applying the Mitra formalism, intracrystalline zeolitic diffusivities with a so far unattained accuracy of a few percents could be obtained. Measurements of such high accuracies are of extreme importance for future activities in elucidating the origin of the discrepancy between the results of different experimental techniques of diffusion measurement in zeolites ⁴.

ACKNOWLEDGEMENTS

The financial support of the German Science Foundation is gratefully acknowledged. J.K. and R.S. are also grateful to the Humboldt-Foundation, the Fonds der Chemischen Industrie, and the Northwestern University, Institute for Environmental Catalysis, for financial support. Thanks are also due to George T. Kokotailo for providing us with faujasite zeolite and to Yoo Joong King for the sample preparation.

REFERENCES

- ¹ N. Y. Chen, T. F. Degnan, and C. M. Smith, *Molecular Transport and Reaction in Zeolites*, VCH ed. (New York, 1994).
- ² L. A. Clark, G. T. Ye, and R. Q. Snurr, *Phys. Rev. Lett.* **84** (13), 2893 (2000); C. Rödenbeck and J. Kärger, *J. Chem. Phys.* **110** (8), 3970 (1999); C. Saravanan and S. M. Auerbach, *J. Chem. Phys.* **110** (22), 11000 (1999).
- ³ J. Kärger and D. M. Ruthven, in *Handbook of Porous Solids*, edited by F. Schüth, K. S. W. Sing, and J. Weitkamp (Wiley-VCH, Weinheim, 2002), p. 2089.
- ⁴ J. Kärger and D. M. Ruthven, *Diffusion in Zeolites and Other Microporous Solids*. (Wiley & Sons, New York, 1992).
- ⁵ J. Kärger and F. Stallmach, in *Diffusion in Condensed Matter: From the Elementary Step to Transport in Complex Systems.*, edited by P. Heitjans and J. Kärger (Springer, Heidelberg, 2003), p. in press.
- ⁶ H. Jobic, in *Recent Advances in Gas Separation by Microporous Ceramic Membranes*, edited by N. K. Kanellopoulos (Elsevier, Amsterdam, 2000), p. 109.
- ⁷ J. Kärger, *Langmuir* **4**, 1289 (1988).
- ⁸ P. H. Nelson and S. M. Auerbach, *Chem. Eng. J.* **74**, 43 (1999).
- ⁹ G. Arya, E. J. Maginn, and H. C. Chang, *J. Phys. Chem. B.* **105** (14), 2725 (2001); M. Chandross, E. B. Webb, G. S. Grest, M. G. Martin, A. P. Thompson, and M. W. Roth, *J. Phys. Chem. B* **105**, 5700 (2001).
- ¹⁰ H. Tanaka, S. Zheng, A. Jentys, and J. A. Lercher, in *Studies of Surface Science and Catalysis*, Vol. 142, p. 1619.
- ¹¹ P. T. Callaghan, *Principles of NMR Microscopy*. (Clarendon Press, Oxford, 1991).
- ¹² R. Kimmich, *NMR Tomography, Diffusometry, Relaxometry*. (Springer, Berlin, 1997).

- 13 J. Crank, *Mathematics of Diffusion*. (Oxford, 1956); S. Chandrasekhar, *Rev. Modern Phys.* **15**, 1 (1943).
- 14 J. Kärger, H. Pfeifer, and W. Heink, *Adv. Magn. Reson.* **12**, 2 (1988).
- 15 P. P. Mitra, P. N. Sen, and L. M. Schwartz, *Phys. Rev. B* **47**, 8565 (1993); P. P. Mitra and P. N. Sen, *Phys. Rev. B* **45**, 143 (1992); P. P. Mitra, P. N. Sen, L. M. Schwartz, and P. LeDoussal, *Phys. Rev. Lett.* **68**, 3555 (1992).
- 16 J. Kärger, M. Petzold, H. Pfeifer, S. Ernst, and J. Weitkamp, *J. Catal.* **136**, 283 (1992).
- 17 S. Frey, J. Kärger, H. Pfeifer, and P. Walther, *J. Magn. Res.* **79**, 336 (1988).
- 18 F. Courivaud, E. W. Hansen, A. Karlsson, S. Kolboe, and M. Stöcker, *Microporous Mesoporous Mater.* **6**, 327 (2000); F. Courivaud, E. W. Hansen, Kobo, A. Karlson, and M. Stöcker, *Micropor. Mesopor. Mater.* **37**, 223 (2000).
- 19 P. Galvosas, F. Stallmach, G. Seiffert, J. Kärger, U. Kaess, and G. Majer, *J. Magn. Reson.* **151** (2), 260 (2001).
- 20 R. M. Cotts, M. J. R. Hoch, T. Sun, and J. T. Markert, *J. Magn. Reson.* **83**, 252 (1989).
- 21 J. Kärger and A. Walter, *Z. phys. Chem., Leipzig* **255**, 142 (1974).
- 22 R. M. Barrer and S. J. W , *Proc. Roy. Soc. A* **237**, 439 (1956).
- 23 J. Kärger, *AIChE J.* **28**, 417 (1982).
- 24 F. Stallmach, C. Vogt, J. Kärger, K. Helbig, and F. Jacobs, *Phys. Rev. Lett.* **88**, 105505 (2002).
- 25 D. N. Theodorou, R. Q. Snurr, and A. T. Bell, in *Comprehensive Supramolecular Chemistry*, edited by G. Alberti and T. Bein (Oxford, 1996), p. 507.

Tables

	$D_0 / \text{m}^2\text{s}^{-1}$	$R / \mu\text{m}$	$(\text{O}(2)/\text{O}(1))_{t_{min}}$	$(\text{O}(2)/\text{O}(1))_{t_{max}}$
2 <i>n</i> -hexane/cav., single component adsorption, 298 K	3.53×10^{-10}	9.1	0.080	0.196
1 <i>n</i> -hexane/cav., two- component adsorption, 298 K	5.54×10^{-10}	7.8	0.070	0.197
1 tetrafluoromethane/cav., two- component adsorption, 203 K	4.17×10^{-10}	9.1	0.240	0.721

Table I. Estimate of the genuine intracrystalline diffusivities (D_0) and the crystal radii (R) by PFG NMR data analysis on the basis of the Mitra formalism (Eqs. (9) and (10) and Refs. ¹⁵). The two last columns represent the ratio of the contributions in second and first order in Eqs. (9) and (10) for the shortest and largest observation times considered in Fig. 6.

Figure Captions

Fig. 1. Scanning electron micrograph (1a) and (volume-weighted) distribution of the crystal radii (1b) of the investigated sample of zeolite NaX.

Fig. 2. PFG NMR signal attenuation curves for *n*-hexane in the two-component sample measured at $T = 298$ K, $t = 500$ (□) and 800 ms (○). Analysis of the data using Eq. (3) yields a root mean square crystal radius of 11.6 μm and 11.9 μm, respectively.

Fig. 3. PFG NMR spin echo attenuation of tetrafluoromethane measured at $T = 203$ K with $t \equiv (\Delta - \tau/2 - \delta/6) = 1.63$ ms (□), 3.63 ms (○), 5.63 ms (Δ), 7.63 ms (◇) and 14.63 ms (∇). The solid lines represent the best fit using a two-exponential fitting function with the amount of molecules $\gamma(t)$ remaining in the crystallite, the intracrystalline diffusivity $D(t)$ and the diffusivity of the molecules leaving the crystallites as fitting parameters.

Fig. 4. NMR tracer desorption curve. The diagram displays the relative contribution $\gamma(t)$ of the second, more slowly decaying part of the spin-echo attenuation curve as presented in Fig. 3 versus the observation time t . The values were obtained by performing two-exponential fits, which are presented in Fig. 3.

Fig. 5. PFG NMR spin echo attenuation of *n*-hexane in the two-component sample measured at $T = 298$ K with $t \equiv (\Delta - \tau/2 - \delta/6) = 1.63$ ms (□), 4.83 ms (○) and 8.63 ms (Δ).

Fig. 6. Relative effective intracrystalline diffusivities $D(t)/D_0$ as function of $\sqrt{D_0 t}$ for *n*-hexane in the single-component sample (○), in the two-component sample (Δ) and for tetrafluoromethane in the two-component sample (□), respectively. The lines shown in the diagram represent the best fits of Eqs. (9) and (10) to the experimental data of $D(t)$ with D_0 and R as fitting parameters.

Figures with figure captions

Note: Figures on separate sheets follow at the end of the manuscript

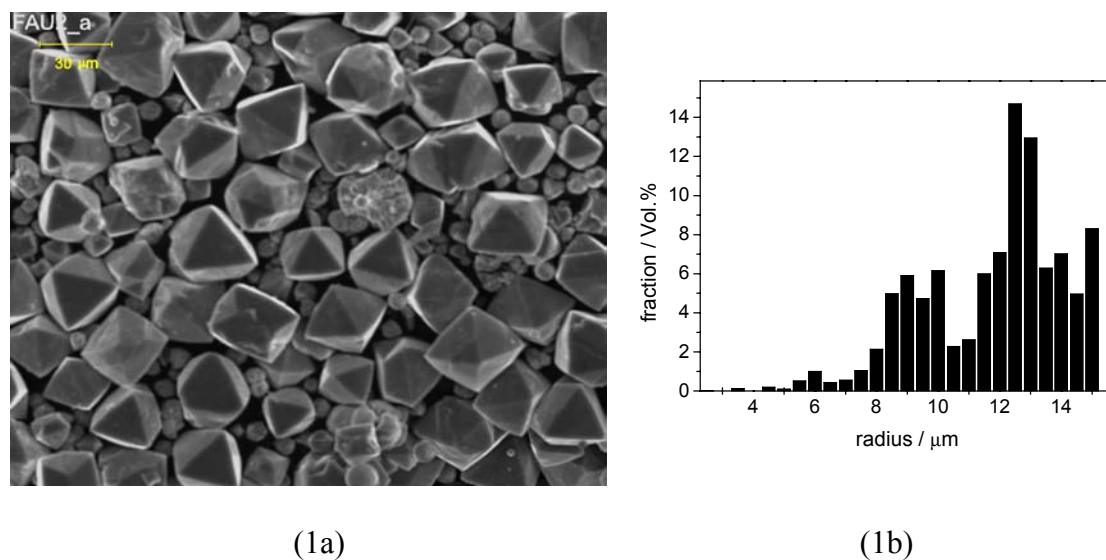


Fig. 1. Scanning electron micrograph (1a) and (volume-weighted) distribution of the crystal radii (1b) of the investigated sample of zeolite NaX.

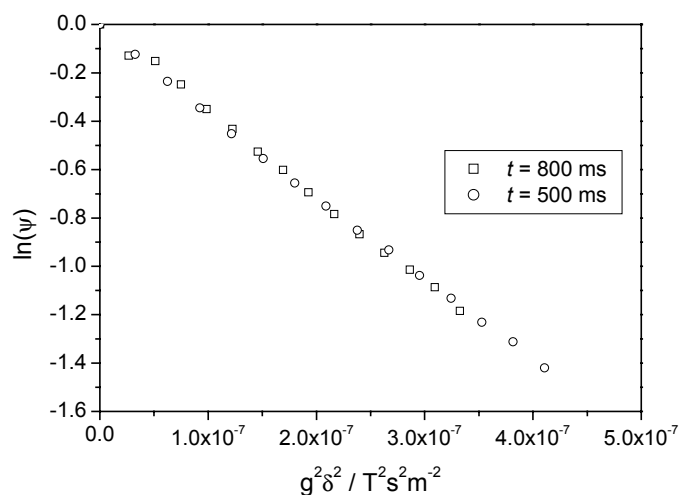


Fig. 2. PFG NMR signal attenuation curves for *n*-hexane in the two-component sample measured at $T = 298$ K, $t = 500$ (□) and 800 ms (○). Analysis of the data using Eq. (3) yields a root mean square crystal radius of 11.6 μm and 11.9 μm, respectively.

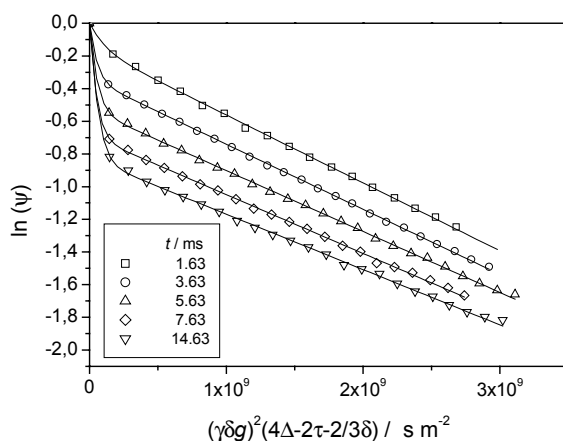


Fig. 3. PFG NMR spin echo attenuation of tetrafluoromethane measured at $T= 203$ K with $t \equiv (\Delta - \tau/2 - \delta/6) = 1.63$ ms (\square), 3.63 ms (\circ), 5.63 ms (Δ), 7.63 ms (\diamond) and 14.63 ms (∇). The solid lines represent the best fit using a two-exponential fitting function with the amount of molecules $\gamma(t)$ remaining in the crystallite, the intracrystalline diffusivity $D(t)$ and the diffusivity of the molecules leaving the crystallites as fitting parameters.

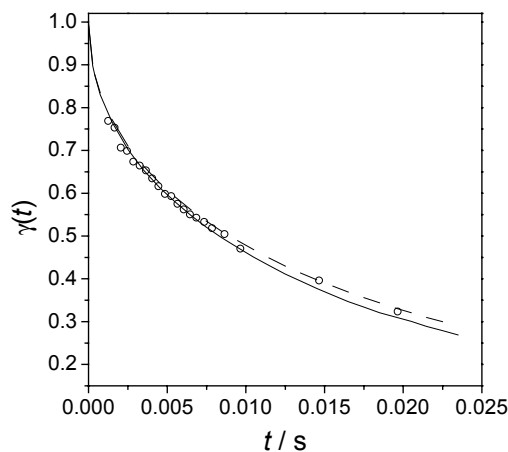


Fig. 4. NMR tracer desorption curve. The diagram displays the relative contribution $\gamma(t)$ of the second, more slowly decaying part of the spin-echo attenuation curve as presented in Fig. 3 versus the observation time t . The values were obtained by performing two-exponential fits, which are presented in Fig. 3.

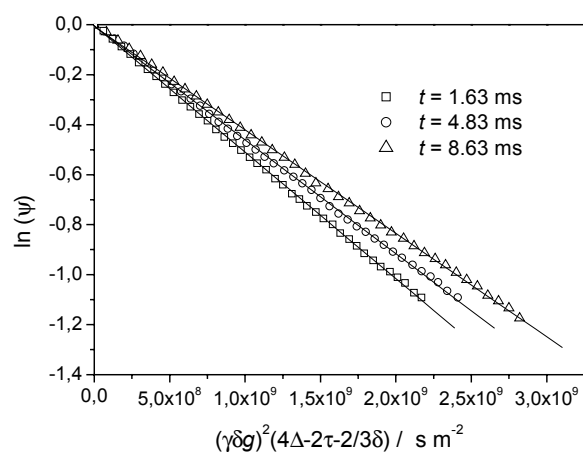


Fig. 5. PFG NMR spin echo attenuation of *n*-hexane in the two-component sample measured at $T=298$ K with $t \equiv (\Delta - \tau/2 - \delta/6) = 1.63$ ms (\square), 4.83 ms (\circ) and 8.63 ms (\triangle).

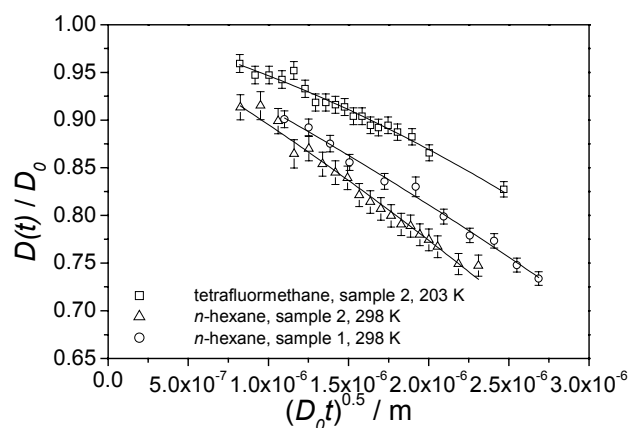
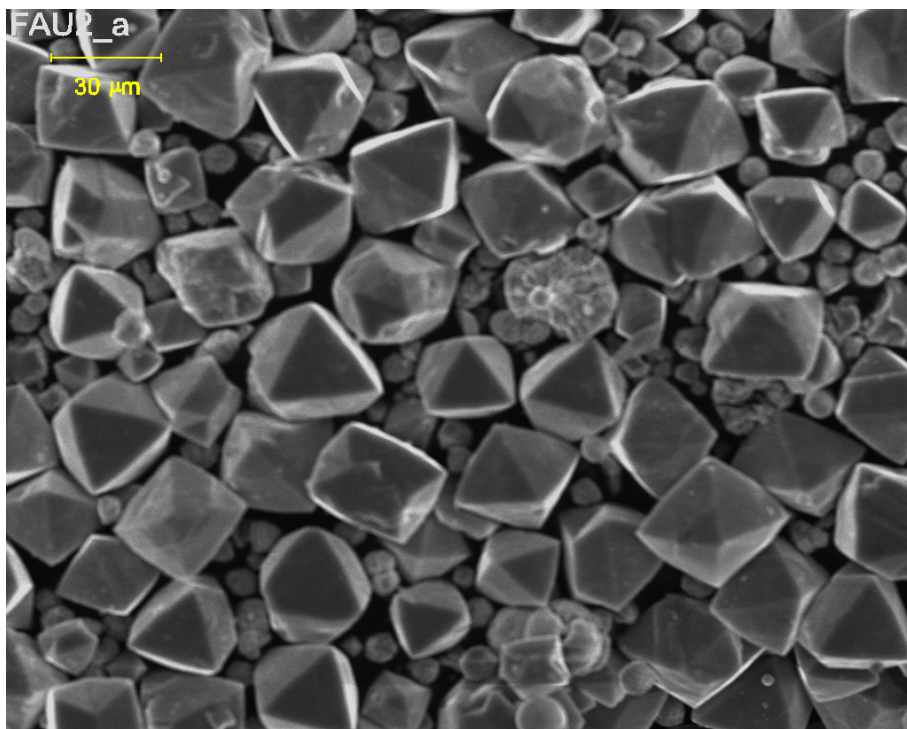
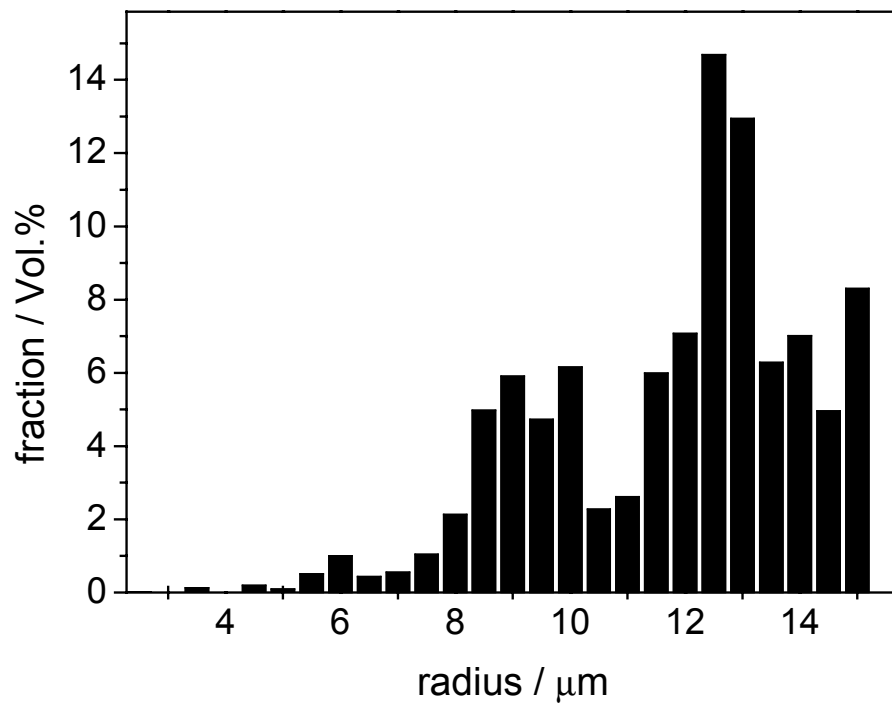


Fig. 6. Relative effective intracrystalline diffusivities $D(t)/D_0$ as function of $\sqrt{D_0 t}$ for *n*-hexane in the single-component sample (\circ), in the two-component sample (\triangle) and for tetrafluoromethane in the two-component sample (\square), respectively. The lines shown in the diagram represent the best fits of Eqs. (9) and (10) to the experimental data of $D(t)$ with D_0 and R as fitting parameters.

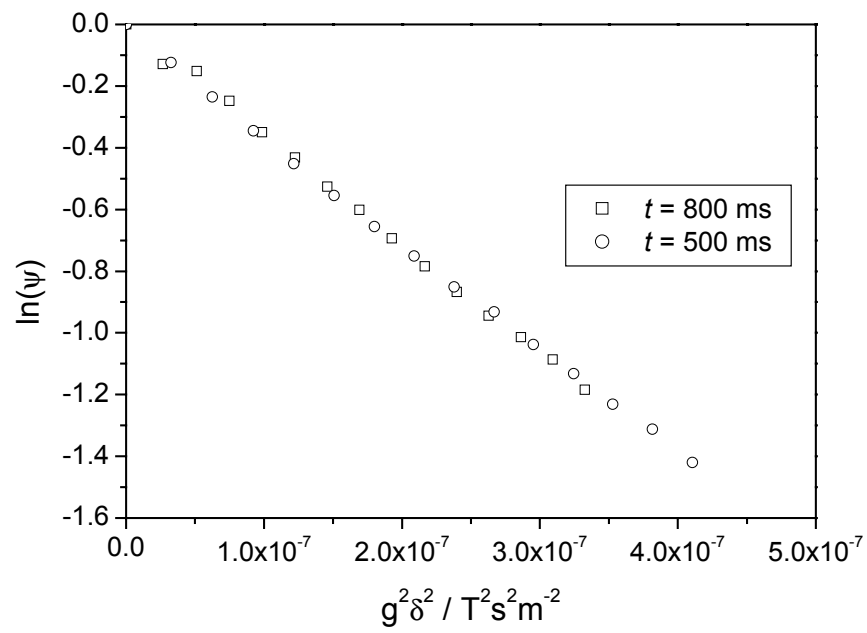
Figures



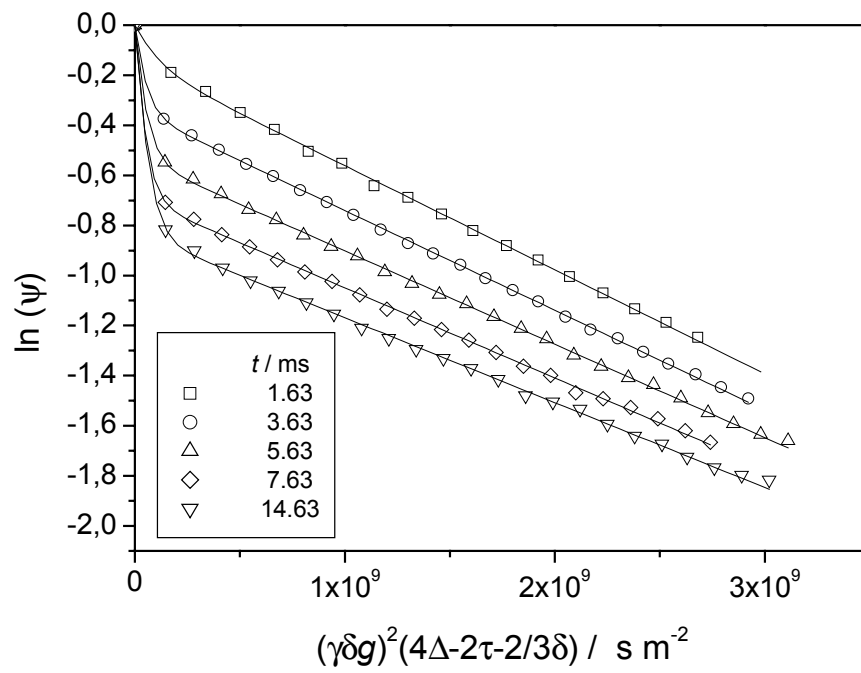
O. Geier et al., Fig. 1a



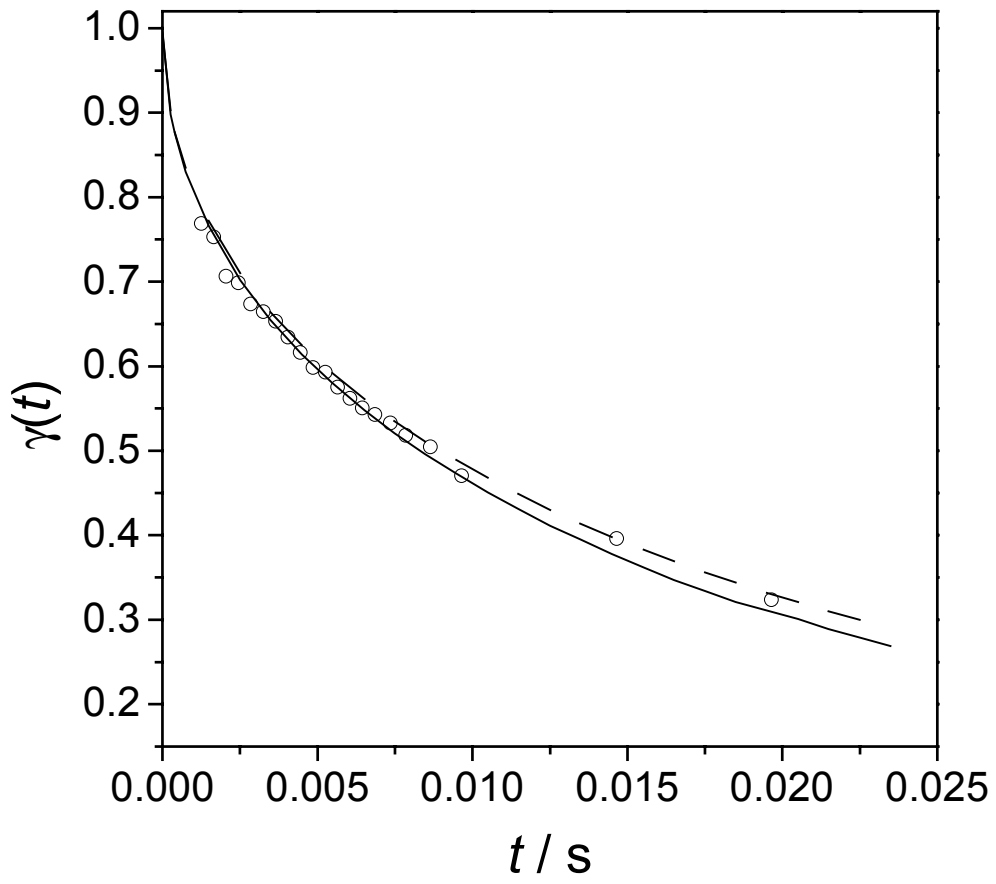
O. Geier et al., Fig. 1b



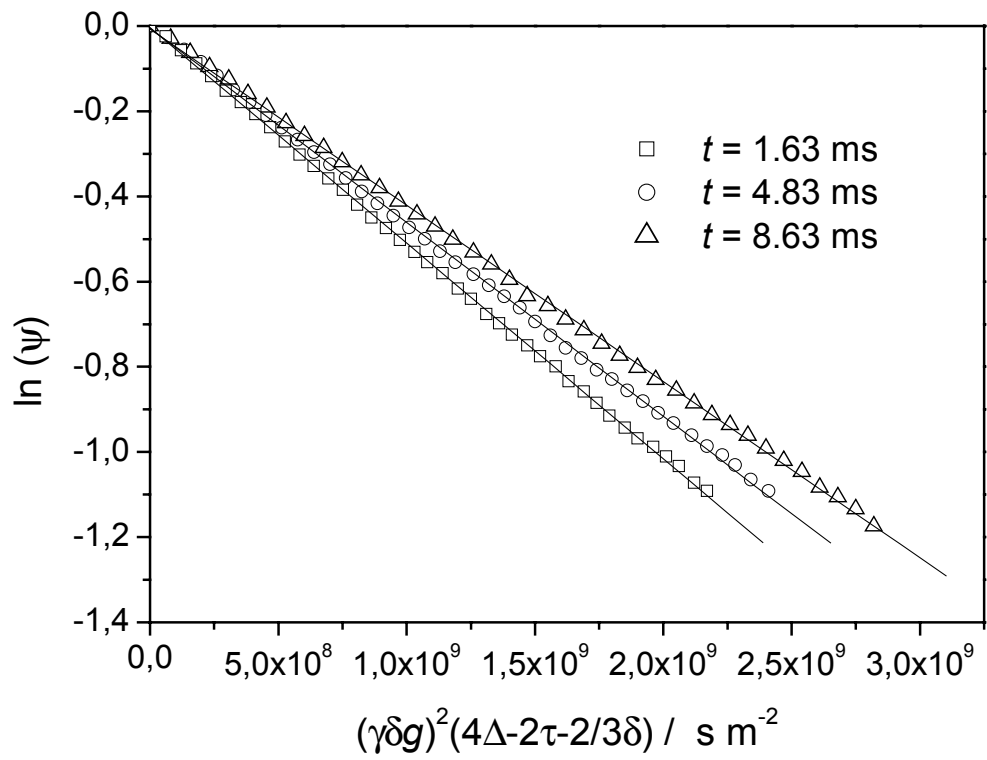
O. Geier et al., Fig. 2



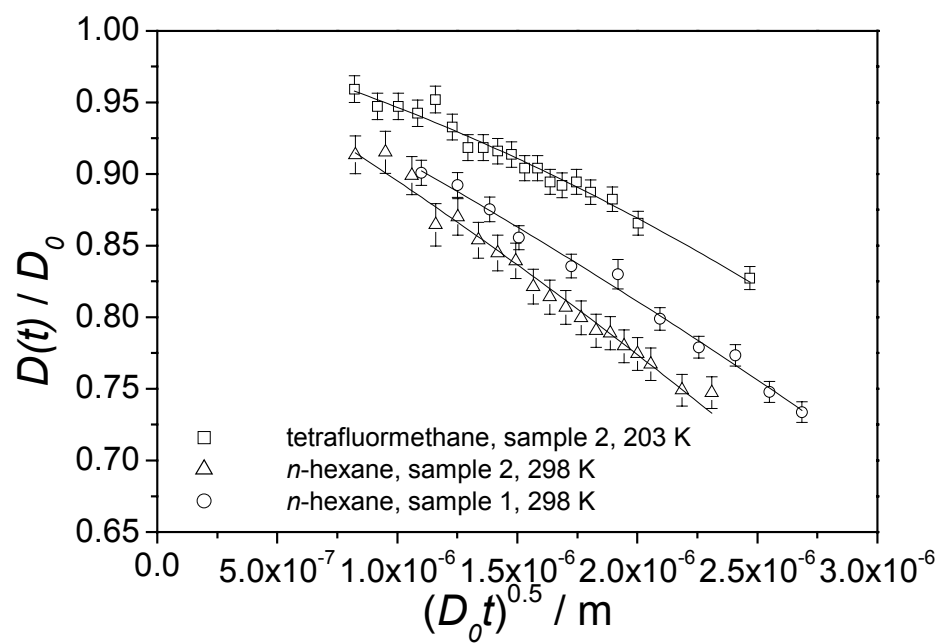
O. Geier et al., Fig. 3



O. Geier et al., Fig. 4



O. Geier et al., Fig. 5



O. Geier et al., Fig. 6